

Shaped-Beam Subarrays for Equi-Power Urban Area Coverage With Modularity and Low Cost

Zhao, Changxu; Yarovoy, Alexander; Roederer, Antoine; Aslan, Yanki

DOI

[10.23919/EuCAP57121.2023.10132931](https://doi.org/10.23919/EuCAP57121.2023.10132931)

Publication date

2023

Document Version

Final published version

Published in

17th European Conference on Antennas and Propagation, EuCAP 2023

Citation (APA)

Zhao, C., Yarovoy, A., Roederer, A., & Aslan, Y. (2023). Shaped-Beam Subarrays for Equi-Power Urban Area Coverage With Modularity and Low Cost. In *17th European Conference on Antennas and Propagation, EuCAP 2023* (pp. 1-5). (17th European Conference on Antennas and Propagation, EuCAP 2023). IEEE. <https://doi.org/10.23919/EuCAP57121.2023.10132931>

Important note

To cite this publication, please use the final published version (if applicable). Please check the document version above.

Copyright

Other than for strictly personal use, it is not permitted to download, forward or distribute the text or part of it, without the consent of the author(s) and/or copyright holder(s), unless the work is under an open content license such as Creative Commons.

Takedown policy

Please contact us and provide details if you believe this document breaches copyrights. We will remove access to the work immediately and investigate your claim.

Green Open Access added to TU Delft Institutional Repository

'You share, we take care!' - Taverne project

<https://www.openaccess.nl/en/you-share-we-take-care>

Otherwise as indicated in the copyright section: the publisher is the copyright holder of this work and the author uses the Dutch legislation to make this work public.

Shaped-Beam Subarrays for Equi-Power Urban Area Coverage With Modularity and Low Cost

Changxu Zhao¹, Alexander Yarovoy², Antoine Roederer³, Yanki Aslan⁴
Microwave Sensing, Signals and Systems Group, Department of Microelectronics,
Faculty of Electrical Engineering, Mathematics, and Computer Science,
Delft University of Technology, Delft, The Netherlands

¹C.Zhao-6@student.tudelft.nl, {²A.Yarovoy, ³A.G.Roederer, ⁴Y.Aslan}@tudelft.nl

Abstract—Design of millimeter-wave arrays for base stations operating in dense urban environment is investigated. Innovative designs for linear subarrays with shaped beam patterns for hybrid beamforming are proposed. The number of elements and element spacings in the subarrays are optimally selected based on a pattern matching technique. The subarrays are designed and verified in series edge-fed slotted substrate integrated waveguide technology at 26 GHz. A novel phase shifter unit is proposed to reduce the subarray width for grating lobe-free beam steering in the plane orthogonal to the sub-array axis. Infinite array simulations are performed to observe the coupling effects on the subarrays.

Index Terms—5G base station, hybrid beamforming, pattern shaping, phased array antenna, substrate integrated waveguide.

I. INTRODUCTION

Multibeam base station antennas will play a key role in mobile communication networks for 5G and beyond which require increased spatial multiplexing and capacity [1]. The ultimate goal is to have fully digital beamforming with the largest flexibility and versatility [2]. However, such approach leads to high costs, heat generation and power consumption which is not yet compatible with the mass market telecom services.

In the recent years, hybrid beamforming solutions have gained more attention due to their appealing cost and performance [3]. In such techniques, subarrays with analog beam control are combined in an array with digital beamforming. Such hybrid beamforming decreases the number of converter chains and the processing complexity at the expense of possible limitations in the field-of-view [4]. A particular approach in hybrid beamforming is to apply analog and digital beamforming separately in the two planes of a radiation diagram (i.e. elevation and azimuth) by employing linear subarrays [5]. Moreover, the subarray beam can be made fixed and shaped for a dedicated application for further complexity reduction and possible system performance improvement [6].

In 5G mm-wave applications, two communication schemes are envisioned [7], which are visualized in Fig. 1. For sub-urban type environments as in Fig. 1(a), the above-mentioned hybrid beamforming idea was exploited recently, for equalized received power at the users independent from their distance, through a classical cosecant-square shaped fixed elevation gain pattern [8]. The pattern was obtained by realizing the



Fig. 1. Common 5G mm-wave communication schemes [7]: (a) sub-urban environments, (b) dense urban environments.

required amplitude and phase distribution in a low-loss series-fed substrate integrated waveguide (SIW) array [9]. In this case, the antenna is located at a large height, a single sided cosecant-squared beam pattern is used to serve roof antennas at multiple houses at similar heights, and digital beamforming is applied in azimuth for multiple steerable beams.

In dense urban environments as in Fig. 1(b), on the other hand, serving both the ground users (cars, pedestrians) and buildings is desired. The single-sided cosecant beam does not work anymore and we need alternative beam shapes in elevation. To the authors' knowledge, this topic has never been investigated in the literature.

In this paper, we propose innovative shaped beam patterns tailored to two representative urban area deployment scenarios. The excitation coefficients for the patterns are smartly obtained for the optimal number of elements and element spacing in terms of pattern matching. The subarrays are realized by applying the series edge-fed SIW slot array design strategy employing a novel phase shifter unit for width reduction. The rest of the paper is organized as follows. Section II describes the array deployment scenarios studied in the paper. Section III explains the pattern synthesis approach. Section IV discusses the subarray design procedures. Section V presents the simulation results including infinite array simulation to investigate subarray behavior under mutual coupling conditions. The conclusions are given in Section VI.

II. ARRAY DEPLOYMENT SCENARIOS

We consider two representative scenarios for urban area service. Scenario-1 is street deployment, while Scenario-2 roundabout or city square deployment. Scenario-1 is visualized in Fig. 2(a). In this case, the antenna panel is orthogonal to the

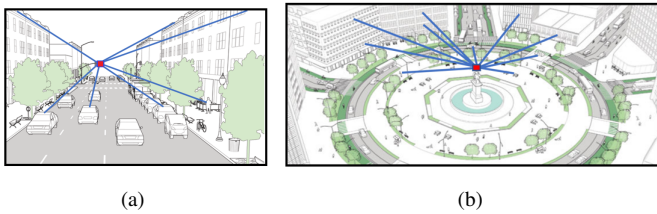


Fig. 2. Urban area base station deployment: (a) Scenario-1: street, (b) Scenario-2: roundabout or city square. (Images are adopted from *nacto.org*)

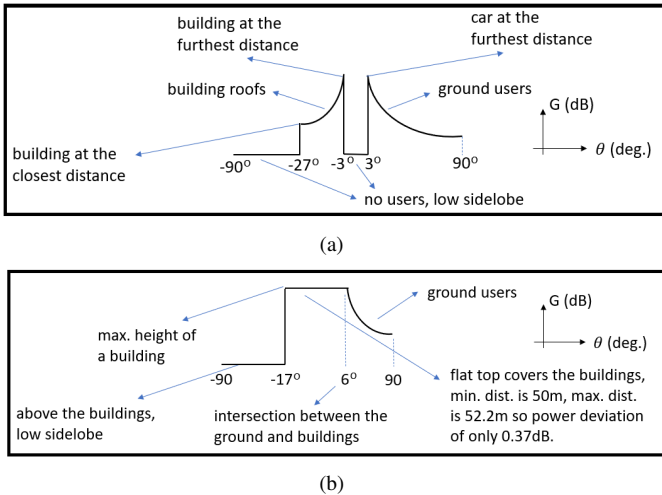


Fig. 3. Shaped elevation beam patterns for the deployment scenarios: (a) Scenario-1, dual-cosecant-squared shape, (b) Scenario-2, combined flat-top cosecant-squared shape.

road. It is located at mid-height as compared to the buildings (e.g. next to the traffic light in the picture) and aims to serve (i) constant-height ground users and (ii) constant-height roof antennas on top of buildings. Our assumptions on the dimensions are as follows. Antenna height: 5m, building roof: 10m, road width: 20m, cell range: 100m. For equi-power service under these assumptions, a dual-cosecant-squared shaped pattern is proposed. The pattern characteristics and relation to the scenario are described in Fig. 3(a).

Scenario-2 is visualized in Fig. 2(b). Similar to Scenario-1, the antenna panel is orthogonal to the road, located at mid-height of the buildings (e.g. on top of a statue in the picture) and aims to serve (i) constant-height ground users and (ii) users at different floors in the buildings. Our assumptions on the dimensions are as follows. Antenna height: 5m, maximal building height: 20m, cell diameter: 100m. For equi-power service under these assumptions, a combined flat-top cosecant-squared pattern is proposed. The pattern characteristics and relation to the scenario are explained in Fig. 3(b).

III. SHAPED PATTERN SYNTHESIS

With low thickness requirements and array layout uniformity, series edge-fed antennas are often preferred despite the potential frequency scanning [9]. For edge-feeding and asymmetrically tapered amplitudes, the pattern phase plays a key role. Here, the synthesis algorithm in [6] which is based

on iterative rephasing and projection of the wanted pattern is used to compute the excitation coefficients. The wanted patterns (masks) are as shown in Fig. 3, with the side lobe level set to -30 dB as compared to the peak gain.

The optimization process was divided into two steps. First, the patterns for varying number of elements with fixed $0.5\lambda_0$ spacing were compared with the mask, which will lead to the optimized number of elements. Second, the pattern matching under different element spacings was performed with the chosen number of elements from the first step. To evaluate the curve matching between the wanted and the simulated patterns, the following equation was used (in dB values):

$$dif. = \text{mean}[(\text{pattern}_{\text{wanted}} - \text{pattern}_{\text{simulated}})^2] \quad (1)$$

After performing the two steps, the number of elements and element spacing are selected, and desired excitation coefficients are obtained under no mutual coupling assumption.

A. Subarray Optimization for Scenario-1

Fig. 4(a) shows the relationship between the curve matching and the number of elements under fixed $0.5\lambda_0$ spacing. Based on this and by considering the trade-off with the subarray length, 12 elements are used. Fig. 4(b) shows the relationship between the curve matching and the element spacing with 12 elements. It was observed that the matching reached the optimum value at $0.65\lambda_0$ spacing. Thus, a 12-element array with $0.65\lambda_0$ spacing was chosen for Scenario-1. Fig. 5(a) shows the comparison between the targeted pattern and the synthesized pattern. Fig. 5(b) shows the required phase and amplitude distribution for the array.

B. Subarray Optimization for Scenario 2

Fig. 4(a) shows the curve matching under fixed $0.5\lambda_0$ spacing for different number of elements. It can be observed

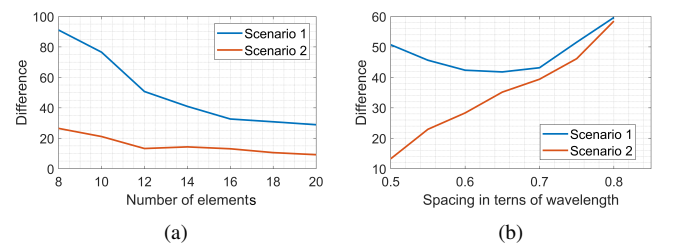


Fig. 4. Pattern matching performance in Scenario-1 for: (a) varying number of element with $0.5\lambda_0$ spacing; (b) varying element spacing with 12 elements.

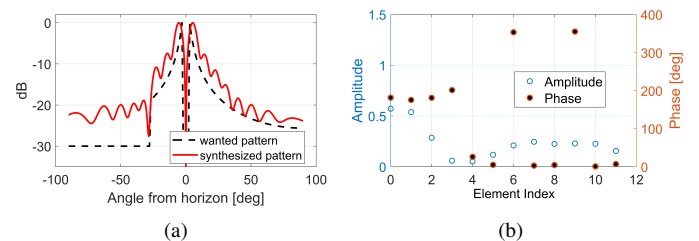


Fig. 5. Array optimization results for Scenario-1: (a) synthesized pattern, (b) phase and amplitude distribution.

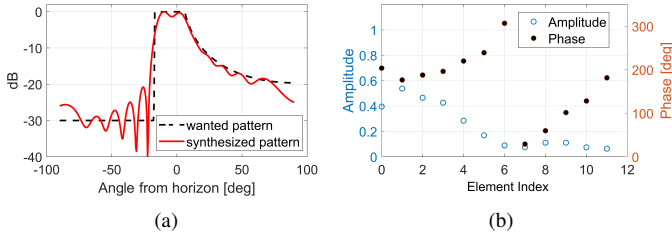


Fig. 6. Array optimization results for Scenario-2: (a) synthesized pattern, (b) phase and amplitude distribution.

that the matching improves at 12 elements and has limited variation between 12 and 20 elements. Fig. 4(b) shows that the curve matching for 12 elements and different element spacings becomes worse when increasing the spacing. Based on these results, a 12-element array with $0.5\lambda_0$ spacing was chosen for Scenario-2. Fig. 6(a) shows the comparison between the targeted pattern and the synthesized pattern. Fig. 6(b) shows the required phase and amplitude distribution.

IV. SUBARRAY DESIGN

A. Unit Cell Structure

The slotted SIW structure shown in Fig. 7 was first proposed in [10] and is further developed in this paper to realize the innovative patterns from Section III. The vias on the side of the waveguide are replaced by continuous PEC walls for fast simulation. A dielectric substrate with $\epsilon_r = 3.37$ is selected for Scenario 1 as in [10], while for Scenario 2, a higher relative permittivity $\epsilon_r = 6.5$ is used to adapt to the larger phase shift requirements in the optimization. The fixed parameters of the designs are shown in Table I. The last element of the subarray is a matched load with the same structure as shown in Fig. 7(a), but using the conducting wall instead at port 2. The modeling and simulation process were done in CST Microwave Studio.

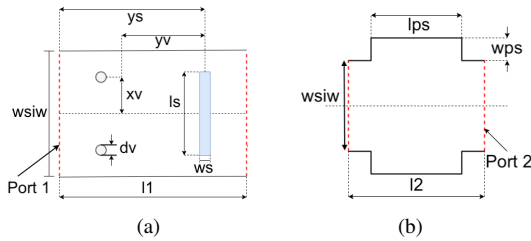


Fig. 7. Structure of the unit cell for flexible excitation: (a) amplitude control unit, (b) phase control unit.

TABLE I
FIXED DESIGN PARAMETERS FOR A UNIT CELL, IN MM

	Scenario 1	Scenario 2
Substrate thickness t_{sub}	0.76	0.76
Substrate permittivity ϵ_r	3.37	6.5
d_v	0.3	0.3
l_1	3.6	2.5
l_2	3.875	3.25
l_{ps}	3.475	2.85
W_c	0.35	0.35
W_{siw}	4.7	3.4
y_s	3	3

During the design, each unit cell was tuned using the optimizer in CST to realize the required amplitude and phase distribution. For convenience, the amplitude was converted into the coupling coefficient using Equations (2) and (3), where $A(n)$ is the excitation coefficient of the n -th element.

$$C = \frac{P_{rad}}{P_{in}} = \frac{1 - |S_{11}|^2 - |S_{21}|^2}{1 - |S_{11}|^2} \quad (2)$$

$$C(n) = \frac{|A(n)|^2}{\sum_{i=1}^N |A(i)|^2} \quad (3)$$

The length of the slot l_s was used to control the value of coupling coefficient with some impact on the phase. The width of the phase shifter section W_{ps} (can be negative as well by definition) and the radius of the vias d_v were used to control the amount of phase shift. The parameters x_v and y_v were used to match the element to the desired frequency (26 GHz).

B. Additional Phase Shifter

The phase shifter structure shown in Fig. 7(b) can change the amount of phase shift by varying the width W_{ps} . However, when a large phase shift is needed, the width for the phase shift increases such that the spacing between the sub-arrays reaches up to λ_0 , leading to grating lobe problems. To reduce the subarray width, additional dielectric vias were added to the structure to bring extra phase shift as shown in Fig. 8. A similar structure has been posed in [11] by using air holes. Here, the amount of phase shift can be controlled by varying the radius of the holes and changing the material filling into the holes as proposed in [12].

V. SIMULATION RESULTS

A. Results for Scenario-1

The tuning results of the unit cells with additional phase shifter were shown in Fig. 9. The dependence on frequency can also be observed. The optimized design parameters for each cell are listed in Table II. The dielectric material with $\epsilon_r = 20$ was used for filling the dielectric vias and the spacing between them was set to be 0.6 mm.

The model of the transverse slot sub-array for Scenario-1 is shown in Fig. 10. The coax-to-SIW feeding was added in the front, the specifications of the feeding structure can be found in [10]. The parameters of the coax-to-SIW transition were optimized together with the sub-array. The simulated (realized) pattern and the reflection coefficient are shown in Fig. 11. The maximum difference between the pattern with and without mutual coupling is around 5 dB at $\theta = \pm 50$ deg. The

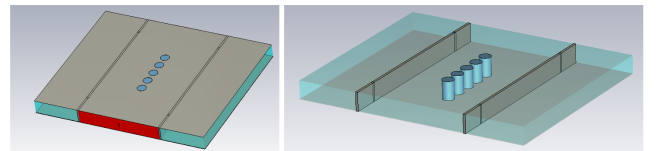


Fig. 8. Structure of the additional phase shifter.

TABLE II
PARAMETERS OF SUB-ARRAY ELEMENTS FOR SCENARIO-1, IN MM

n	l_s	x_v	y_v	W_{ps}	dv_{hole}
1	3.392	1.297	2.33	0	0.3
2	3.533	1.251	2.061	0	0.457
3	2.291	1.368	2.081	0	0.4
4	2.268	1.473	0.936	-0.648	0.312
5	2.076	1.792	2.566	0	0.561
6	2.664	1.622	2.288	0	0.483
7	3.162	1.429	2.109	0	0.371
8	3.316	1.344	2.11	0	0.415
9	3.322	1.324	2.136	0	0.474
10	3.514	1.258	2.066	0	0.4
11	3.759	1.172	2.001	0	0.417
12	3.94	1.119	1.987	0	

maximum directivity of the realized pattern is 2.3 dB lower than the synthesized pattern without coupling.

In case of a infinite linear array of subarrays, the behaviour of the subarray for different spacing along x-direction is shown in Fig. 12. The reflection coefficient at 26 GHz is below -10 dB under the sub-array spacing from $0.5\lambda_0$ to $0.8\lambda_0$. Besides, the maximum directivity increased from 12.58 dB to 14.49 dB when increasing the sub-array spacing from $0.5\lambda_0$ to $0.8\lambda_0$. The behaviour of the infinite array under different scanning angles at fixed $0.5\lambda_0$ sub-array spacing is shown in Fig. 13(a). The reflection coefficient at 26 GHz is below -10 dB except for the scanning angles at 0 deg and 60 deg. The embedded subarray patterns for the finite 7-subarrays

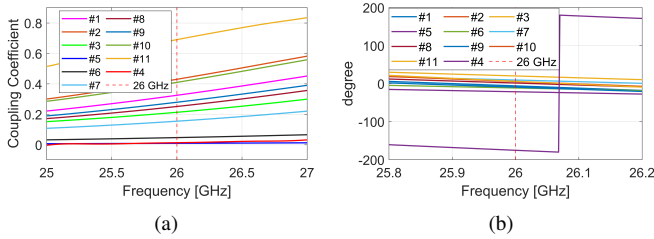


Fig. 9. Element tuning results for Scenario-1: (a) coupling coefficient, (b) phase shift.

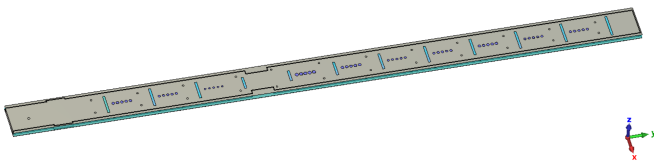


Fig. 10. Transverse slot sub-array for Scenario-1.

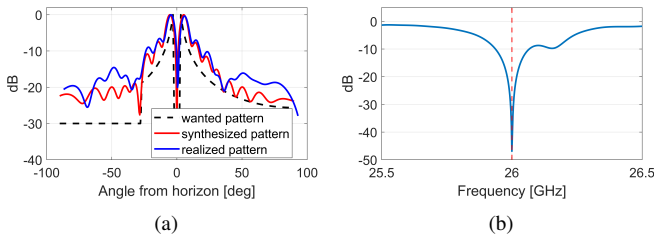


Fig. 11. Subarray performance for Scenario-1: (a) simulated pattern, (b) reflection coefficient.

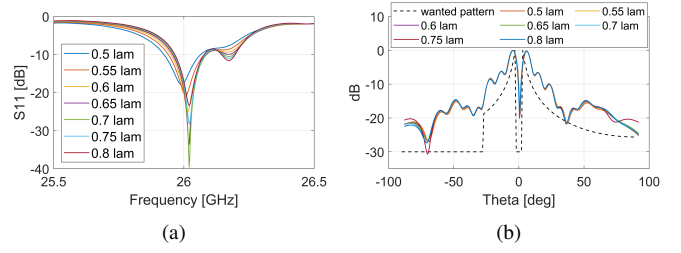


Fig. 12. Infinite array simulation results for different sub-array spacing in Scenario-1: (a) reflection coefficient, (b) radiation pattern.

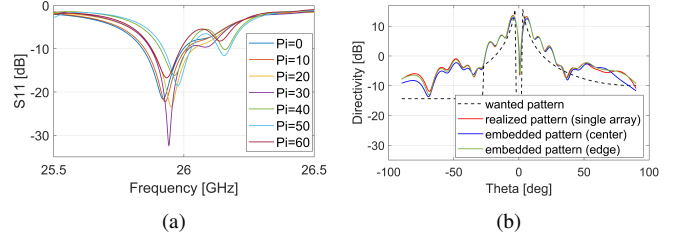


Fig. 13. (a) Reflection coefficient of the infinite array simulation for different scan angles in Scenario-1 for $0.5\lambda_0$ sub-array spacing, (b) Embedded subarray patterns in the 7-subarrays simulation for $0.5\lambda_0$ sub-array spacing.

simulation are shown in Fig. 13(b). The maximum directivity of the edge-subarray is similar as the single sub-array, while for the center-subarray, the maximum directivity is 0.74 dB lower.

B. Results for Scenario-2

The tuning results of the unit cells are shown in Fig. 14. The optimized parameters for each cell are listed in Table III. The dielectric material with $\epsilon_r = 20$ was used for filling the dielectric vias of the first element. The phase shift vias for elements 2 to 5 were filled in with $\epsilon_r = 10.2$. For elements 6 to 11, the phase shift vias were filled in with air.

The model of the transverse slot subarray for Scenario-2 is shown in Fig. 15. The parameters of the coax-to-siw feeding element are optimized, as in the array from Scenario-1. The simulated (realized) pattern and reflection coefficient are shown in Fig. 16. Due to the mutual coupling, the side lobe around $\theta = -24$ deg is increased by 5 dB. In addition, the maximum directivity of the realized pattern is 1.44 dB lower than the synthesized pattern without coupling.

The simulated results of the infinite array with different sub-array spacing are presented in Fig. 17. The reflection

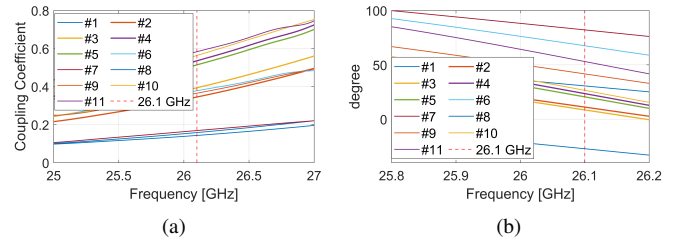


Fig. 14. Element tuning results for Scenario-2: (a) coupling coefficient, (b) phase shift.

TABLE III
PARAMETERS OF SUB-ARRAY ELEMENTS FOR SCENARIO-2, IN MM

n	l_s	x_v	y_v	W_{ps}	dv_{hole}
1	2.563	1.058	1.536	1	0.405
2	2.779	0.962	1.505	0.144	0.3
3	2.815	0.945	1.5	0.217	0.3
4	2.895	0.906	1.492	0	0.3
5	2.882	0.911	1.494	0	0.35
6	2.739	0.983	1.54	-0.173	0.5
7	2.484	1.189	1.633	-0.264	0.5
8	2.552	1.072	1.523	0	0.278
9	2.777	0.959	1.514	0	0.436
10	2.915	0.898	1.486	0.098	0.254
11	2.912	0.896	1.491	-0.163	0.248
12	3.294	0.835	1.397		

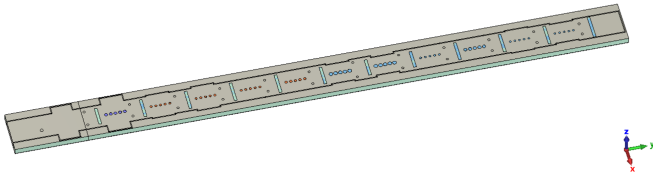


Fig. 15. Transverse slot sub-array for Scenario-2.

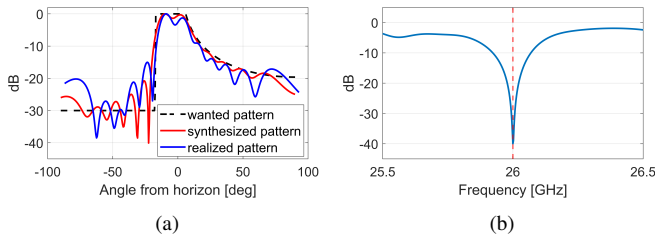


Fig. 16. Subarray performance for Scenario-2: (a) simulated pattern, (b) reflection coefficient.

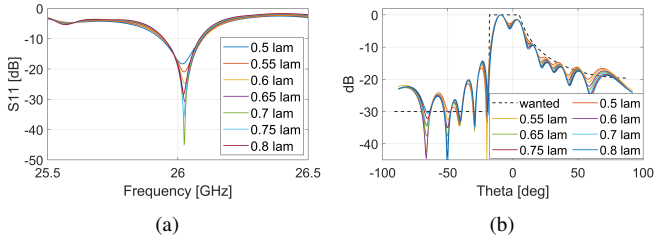


Fig. 17. Infinite array simulation results for different sub-array spacing in Scenario-2: (a) reflection coefficient, (b) radiation pattern.

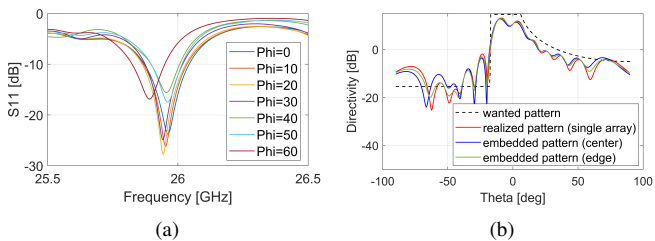


Fig. 18. (a) Reflection coefficient of the infinite array simulation for different scan angles in Scenario-1 for $0.5\lambda_0$ sub-array spacing, (b) Embedded subarray patterns in the 7-subarrays simulation for $0.5\lambda_0$ sub-array spacing.

coefficient at 26 GHz is below -10 dB for the sub-array spacing from $0.5\lambda_0$ to $0.8\lambda_0$. The reflection coefficient of the infinite array under different scan angles is shown in Fig. 18(a). The reflection coefficient at 26 GHz is below -10 dB until reaching the 60 deg scan angle. The embedded subarray patterns for the finite 7-subarrays simulation are presented in Fig. 18(b). Both center and edge subarrays show similar maximum directivity as the single isolated subarray, while the edge element has slightly lower side-lobe levels as compared to the center element.

VI. CONCLUSION

Two new transverse slot SIW-fed sub-arrays operating at 26 GHz have been designed to operate in base station antennas with hybrid beamforming dedicated to work in dense urban environments. The radiation patterns in the elevation plane have been tailored to two innovative and representative deployment scenarios: street and roundabout or city square with a unique dual-cosecant-squared and combined flat-top cosecant-squared pattern, respectively. To limit the distance between the sub-arrays and avoid grating lobes while scanning in azimuth, a novel phase shift structure that uses dielectric vias has been proposed and implemented into the sub-array design. The impedance and pattern matching performance of the sub-arrays have been successfully verified in isolated simulation environment. Mutual coupling effects on the active reflection coefficients and beam patterns have also been analyzed via infinite array simulations and have been found to have limited effect on the radiation patterns.

REFERENCES

- [1] W. Hong et al., "Multibeam antenna technologies for 5G wireless communications," *IEEE Trans. Antennas Propag.*, vol. 65, no. 12, pp. 6231-6249, 2017.
- [2] B. Yang et al., "Digital beamforming-based massive MIMO transceiver for 5G millimeter-wave communications," *IEEE Trans. Microw. Theory Techn.*, vol. 66, no. 7, pp. 3403-3418, 2018.
- [3] I. Ahmed et al., "A survey on hybrid beamforming techniques in 5G: architecture and system model perspectives," *IEEE Commun. Surveys Tuts.*, vol. 20, no. 4, pp. 3060-3097, 2018.
- [4] Y. Aslan, J. Puskely, A. Roederer, and A. Yarovoy, "Active multipoint subarrays for 5G communications", in *Proc. IEEE APWC*, pp. 298-303, 2019.
- [5] Y. Hu and W. Hong, "A novel hybrid analog-digital multibeam antenna array for massive MIMO applications", in *Proc. IEEE Asia Pacific Conf. Antennas Propag.*, Auckland, New Zealand, pp. 42-45, 2018.
- [6] A. Roederer, J. Puskely, Y. Aslan and A. Yarovoy, "Shaped elevation patterns for 5G base stations," in *Proc. IEEE AP-SURSI*, Singapore, 2021.
- [7] T. Cameron, "Bits to beams: Rf technology evolution for 5G millimeter wave radios", in *Tech. Art.*, Analog Devices Inc., 2018.
- [8] J. Puskely, Y. Aslan, A. Roederer and A. Yarovoy, "SIW based antenna array with power equalization in elevation plane for 5G base stations", in *Proc. 12th EuCAP*, London, UK, Apr. 2018.
- [9] J. Puskely et al., "5G SIW based phased antenna array with cosecant squared shape pattern," *IEEE Trans. Antennas Propag.*, vol. 70, no. 1, pp. 250-259, 2022.
- [10] T. Mikulasek et al., "Transverse slot with control of amplitude and phase for travelling-wave SIW antenna arrays," *IET Microw. Antennas Propag.*, vol. 14, no. 15, pp. 1943-1946, 2020.
- [11] I. Boudreau, K. Wu and D. Deslandes, "Broadband phase shifter using air holes in Substrate Integrated Waveguide", in *IEEE MTT-S Int. Microw. Symp.*, Baltimore, MD, USA, 2011.
- [12] H. I. Kremer, K. W. Leung and M. W. K. Lee, "Design of Substrate-integrated dielectric resonator antenna with dielectric vias," *IEEE Trans. Antennas Propag.*, vol. 69, no. 9, pp. 5205-5214, 2021.